Z. Phys. C – Particles and Fields 56, 47–61 (1992)

Zeitschrift für Physik C Particles and Fields

Measurement of the partial width of the Z^0 into $b\bar{b}$ final states using their semi-leptonic decays

DELPHI Collaboration

P. Abreu[19], W. Adam[46], T. Adye[34], E. Agasi[28], G.D. Alekseev[13], P. Allen[45], S. Almehed[22], S.J. Alvsvaag[4], U. Amaldi[7], E.G. Anassontzis[3], A. Andreazza[26], P. Antilogus[23], W.-D. Apel[14], R.J. Apsimon[34], B. Åsman[41], J.-E. Augustin[17], A. Augustinus[28], P. Baillon[7], P. Bambade[17], F. Barao[19], R. Barate[11], G. Barbiellini[43], D.Y. Bardin[13], A. Baroncelli[37], O. Barring[22], J.A. Barrio[24], W. Bartl[46], M.J. Bates[31], M. Battaglia[26], M. Baubillier[21], K.-H. Becks[48], C.J. Beeston[31], M. Begalli[33], P. Beilliere[6], Yu. Belokopytov[39], P. Beltran[9], D. Benedic[8], M. Berggren[17], D. Bertrand[2], F. Bianchi[42], M.S. Bilenky[13], P. Billoir[21], J. Bjarne[22], D. Bloch[8], S. Blyth[31], V. Bocci[35], P.N. Bogolubov[13], T. Bolognese[36], M. Bonesini[26], W. Bonivento[26], P.S.L. Booth[20], P. Borgeaud[36], G. Borisov[39], H. Borner[7], C. Bosio[37], B. Bostjancic[7], S. Bosworth[31], O. Botner[44], B. Bouquet[17], C. Bourdarios[17], T.J.V. Bowcock[20], M. Bozzo[10], S. Braibant[2], P. Branchini[37], K.D. Brand[32], R.A. Brenner[7], H. Briand[21], C. Bricman[2], R.C.A. Brown[7], N. Brummer[28], J.-M. Brunet[6], L. Bugge[30], T. Buran[30], H. Burmeister[7], J.A.M.A. Buytaert[2], M. Caccia[7], M. Calvi[26], A.J. Camacho Rozas[38], T. Camporesi[7], V. Canale[35], F. Cao[2], F. Carena[7], L. Carroll[20], C. Caso[10], E. Castelli[43], M.V. Castillo Gimenez[45], A. Cattai[7], F.R. Cavallo[5], L. Cerrito[35], V. Chabaud[7], A. Chan[1], Ph. Charpentier[7], L. Chaussard[17], J. Chauveau[21], P. Checchia[32], G.A. Chelkov[13], L. Chevalier[36], P. Chliapnikov[39], V. Chorowicz[21], J.T.M. Chrin[45], R. Cirio[42], M.P. Clara[42], P. Collins[31], J.L. Contreras[24], R. Contri[10], E. Cortina[45], G. Cosme[17], F. Couchot[17], H.B. Crawley[1], D. Crennell[34], G. Crossetti[10], M. Crozon[6], J. Cuevas Maestro[38], S. Czellar[12], S. Dagoret[17], E. Dahl-Jensen[27], B. Dalmagne[17], M. Dam[30], G. Damgaard[27], G. Darbo[10], E. Daubie[2], A. Daum[14], P.D. Dauncey[31], M. Davenport[7], P. David[21], W. Da Silva[21], C. Defoix[6], D. Delikaris[7], B.A. Della Riccia[42], S. Delorme[7], P. Delpierre[6], N. Demaria[42], A. De Angelis[43], M. De Beer[36], H. De Boeck[2], W. De Boer[14], C. De Clercq[2], M.D.M. De Fez Laso[45], N. De Groot[28], C. De La Vaissiere[21], B. De Lotto[43], A. De Min[26], H. Dijkstra[7], L. Di Ciaccio[35], F. Djama[8], J. Dolbeau[6], M. Donszelmann[7], K. Doroba[47], M. Dracos[7], J. Drees[48], M. Dris[29], Y. Dufour[6], L.-O. Eek[44], P.A.-M. Eerola[7], R. Ehret[14], T. Ekelof[44], G. Ekspong[41], A. Elliot Peisert[32], J.-P. Engel[8], D. Fassouliotis[29], T.A. Fearnley[4], M. Feindt[7], A. Fenyuk[39], M. Fernandez Alonso[38], A. Ferrer[45], T.A. Filippas[29], A. Firestone[1], H. Foeth[7], E. Fokitis[29], F. Fontanelli[10], K.A.J. Forbes[20], B. Franek[34], P. Frenkiel[6], D.C. Fries[14], A.G. Frodesen[4], R. Fruhwirth[46], F. Fulda-Quenzer[17], K. Furnival[20], H. Furstenau[14], J. Fuster[7], G. Galeazzi[32], D. Gamba[42], C. Garcia[45], J. Garcia[38], C. Gaspar[7], U. Gasparini[32], Ph. Gavillet[7], E.N. Gazis[29], J.-P. Gerber[8], P. Giacomelli[7], R. Gokieli[47], B. Golob[40], V.M. Golovatyuk[13], J.J. Gomez Y Cadenas[7], A. Goobar[41], G. Gopal[34], M. Gorski[47], V. Gracco[10], A. Grant[7], F. Grard[2], E. Graziani[37], G. Grosdidier[17], E. Gross[7], P. Grosse-Wiesmann[7], B. Grossetete[21], S. Gumenyuk[39], J. Guy[34], U. Haedinger[14], F. Hahn[48], M. Hahn[14], S. Haider[28], Z. Hajduk[15], A. Hakansson[22], A. Hallgren[44], K. Hamacher[48], G. Hamel De Monchenault[36], W. Hao[28], F.J. Harris[31], T. Henkes[7], J.J. Hernandez[45], P. Herquet[2], H. Herr[7], T.L. Hessing[20], I. Hietanen[12], C.O. Higgins[20], E. Higon[45], H.J. Hilke[7], S.D. Hodgson[31], T. Hofmokl[47], R. Holmes[1], S.-O. Holmgren[41], D. Holthuizen[28], P.F. Honore[6], J.E. Hooper[27], M. Houlden[20], J. Hrubec[46], P.O. Hulth[41], K. Hultqvist[41], P. Ioannou[3], D. Isenhower[7], P.-S. Iversen[4], J.N. Jackson[20], P. Jalocha[15], G. Jarlskog[22], P. Jarry[36], B. Jean-Marie[17], E.K. Johansson[41], D. Johnson[20], M. Jonker[7], L. Jonsson[22], P. Juillot[8], G. Kalkanis[3], G. Kalmus[34], F. Kapusta[21], M. Karlsson[7], E. Karvelas[9], S. Katsanevas[3], E.C. Katsoufis[29], R. Keranen[12], J. Kesteman[2], B.A. Khomenko[13], N.N. Khovanski[13], B. King[20], N.J. Kjaer[7], H. Klein[7], W. Klempt[7], A. Klovning[4], P. Kluit[28], A. Koch-Mehrin[48], J.H. Koehne[14], B. Koene[28], P. Kokkinias[9], M. Kopf[14], K. Korcyl[15], A.V. Korytov[13], V. Kostioukhine[39], C. Kourkoumelis[3], O. Kouznetsov[13], P.H. Kramer[48], J. Krolikowski[47], I. Kronkvist[22], J. Krstic[31], U. Kruener-Marquis[48], W. Krupinski[15], K. Kulka[44], K. Kurvinen[12], C. Lacasta[45], C. Lambropoulos[9], J.W. Lamsa[1], L. Lanceri[43], V. Lapin[39], J.-P. Laugier[36], R. Lauhakangas[12], G. Leder[46], F. Ledroit[11], R. Leitner[7], Y. Lemoigne[36], J. Lemonne[2], G. Lenzen[48], V. Lepeltier[17], J.M. Levy[8], E. Lieb[48], D. Liko[46], E. Lillethun[4], J. Lindgren[12], R. Lindner[48], A. Lipniacka[47], I. Lippi[32], B. Loerstad[22], M. Lokajicek[13], J.G. Loken[31], A. Lopez-Fernandez[17], M.A. Lopez Aguera[38], M. Los[28], D. Loukas[9], J.J. Lozano[45], P. Lutz[6], L. Lyons[31], G. Maehlum[7], J. Maillard[6], A. Maltezos[9], F. Mandl[46], J. Marco[38], M. Margoni[32], J.-C. Marin[7], A. Markou[9], T. Maron[48], S. Marti[45], L. Mathis[1], F. Matorras[38], C. Matteuzzi[26], C. Matthiae[35], M. Mazzucato[32], M. Mc Cubbin[20], R. Mc Kay[1], R. Mc Nulty[20], G. Meola[10], C. Meroni[26], W.T. Meyer[1], M. Michelotto[32], I. Mikulec[46], W.A. Mitaroff[46], G.V. Mitselmakher[13], U. Mjoernmark[22], T. Moa[41], R. Moeller[27], K. Moenig[7], M.R. Monge[10], P. Morettini[10], H. Mueller[14], W.J. Murray[34], B. Muryn[17], G. Myatt[31], F. Naraghi[21], F.L. Navarria[5], P. Negri[26], B.S. Nielsen[27], B. Nijjhar[20], V. Nikolaenko[39], P.E.S. Nilsen[4], P. Niss[41], V. Obraztsov[39], A.G. Olshevski[13], R. Orava[12],

A. Ostankov[39], K. Osterberg[12], A. Ouraou[36], M. Paganoni[26], R. Pain[21], H. Palka[28], Th.D. Papadopoulou[29], L. Pape[7], A. Passeri[37], M. Pegoraro[32], J. Pennanen[12], V. Perevozchikov[39], M. Pernicka[46], A. Perrotta[5], A. Petrolini[10], T.E. Pettersen[32], F. Pierre[36], M. Pimenta[19], O. Pingot[2], M.E. Pol[7], G. Polok[15], P. Poropat[43], P. Privitera[14], A. Pullia[26], D. Radijicic[31], S. Ragazzi[26], P.N. Ratoff[18], A.L. Read[30], N.G. Redaelli[26], M. Regler[46], D. Reid[20], P.B. Renton[31], L.K. Resvanis[3], F. Richard[17], M. Richardson[20], J. Ridky[13], G. Rinaudo[42], I. Roditi[16], A. Romero[42], I. Roncagliolo[10], P. Ronchese[32], C. Ronnqvist[12], E.I. Rosenberg[1], S. Rossi[7], U. Rossi[5], E. Rosso[7], P. Roudeau[17], T. Rovelli[5], W. Ruckstuhl[28], V. Ruhlmann[36], A. Ruiz[38], K. Rybicki[15], H. Saarikko[12], Y. Sacquin[36], G. Sajot[11], J. Salt[45], J. Sanchez[24], M. Sannino[10], S. Schael[14], H. Schneider[14], M.A.E. Schyns[48], G. Sciolla[42], F. Scuri[43], A.M. Segar[31], R. Sekulin[34], M. Sessa[43], G. Sette[10], R. Seufert[14], R.C. Shellard[33], I. Siccama[28], P. Siegrist[36], S. Simonetti[10], F. Simonetto[32], A.N. Sisakian[13], T.B. Skaali[30], G. Skjevling[30], G. Smadja[36,23], G.R. Smith[34], R. Sosnowski[47], T.S. Spassoff[11], E. Spiriti[37], S. Squarcia[10], H. Staeck[48], C. Stanescu[37], S. Stapnes[30], G. Stavropoulos[9], F. Stichelbaut[2], A. Stocchi[17], J. Strauss[46], J. Straver[7], R. Strub[8], M. Szczekowski[47], M. Szeptycka[47], P. Szymanski[47], T. Tabarelli[26], S. Tavernier[2], O. Tchikilev[39], G.E. Theodosiou[9], A. Tilquin[25], J. Timmermans[28], V.G. Timofeev[13], L.G. Tkatchev[13], T. Todorov[8], D.Z. Toet[28], O. Toker[12], E. Torassa[42], L. Tortora[37], M.T. Trainor[31], D. Treille[7], U. Trevisan[10], W. Trischuk[7], G. Tristram[6], C. Troncon[26], A. Tsirou[7], E.N. Tsyganov[13], M. Turala[15], M.-L. Turluer[36], T. Tuuva[12], I.A. Tyapkin[21], M. Tyndel[34], S. Tzamarias[7], S. Ueberschaer[48], O. Ullaland[7], V. Uvarov[39], G. Valenti[5], E. Vallazza[42], J.A. Valls Ferrer[45], C. Vander Velde[2], G.W. Van Apeldoorn[28], P. Van Dam[28], W.K. Van Doninck[2], J. Varela[19], P. Vaz[7], G. Vegni[26], L. Ventura[32], W. Venus[34], F. Verbeure[2], L.S. Vertogradov[13], D. Vilanova[36], L. Vitale[12], E. Vlasov[39], A.S. Vodopyanov[13], M. Vollmer[48], S. Volponi[5], G. Voulgaris[3], M. Voutilainen[12], V. Vrba[37], H. Wahlen[48], C. Walck[41], F. Waldner[43], M. Wayne[1], A. Wehr[48], M. Weierstall[48], P. Weilhammer[7], J. Werner[48], A.M. Wetherell[7], J.H. Wickens[2], J. Wikne[30], G.R. Wilkinson[31], W.S.C. Williams[31], M. Winter[8], D. Wormald[30], K. Woschnagg[44], N. Yamdagni[41], P. Yepes[7], A. Zaitsev[39], A. Zalewska[15], P. Zalewski[17], D. Zavrtanik[7], E. Zevgolatakos[9], G. Zhang[48], N.I. Zimin[13], M. Zito[36], R. Zuberi[31], R. Zukanovich Funchal[6], G. Zumerle[32], J. Zuniga[45]

[1] Ames Laboratory and Department of Physics, Iowa State University, Ames IA 50011, USA
[2] Physics Department, Univ. Instelling Antwerpen, Universiteitsplein 1, B-2610 Wilrijk, Belgium
and IIHE, ULB-VUB, Pleinlaan 2, B-1050 Brussels, Belgium
and Faculté des Sciences, Univ. de l'Etat Mons, Av. Maistriau 19, B-7000 Mons, Belgium
[3] Physics Laboratory, University of Athens, Solonos Str. 104, GR-10680 Athens, Greece
[4] Department of Physics, University of Bergen, Allégaten 55, N-5007 Bergen, Norway
[5] Dipartimento di Fisica, Università di Bologna and INFN, Via Irnerio 46, I-40126 Bologna, Italy
[6] Collège de France, Lab. de Physique Corpusculaire, 11 pl. M. Berthelot, F-75231 Paris Cedex 05, France
[7] CERN, CH-1211 Geneva 23, Switzerland
[8] Centre de Recherche Nucléaire, IN2P3-CNRS/ULP-BP20, F-67037 Strasbourg Cedex, France
[9] Institute of Nuclear Physics, N.C.S.R. Demokritos, P.O. Box 60228, GR-15310 Athens, Greece
[10] Dipartimento di Fisica, Università di Genova and INFN, Via Dodecaneso 33, I-16146 Genova, Italy
[11] Institut des Sciences Nucléaires, Université de Grenoble 1, F-38026 Grenoble, France
[12] Research Institute für High Energy Physics, SEFT, Siltavuorenpenger 20C, SF-00170 Helsinki, Finland
[13] Joint Institute for Nuclear Research, Dubna, Head Post Office, P.O. Box 79, 101 000 Moscow, Russia
[14] Institut für Experimentelle Kernphysik, Universität Karlsruhe, Postfach 6980, W-7500 Karlsruhe 1, Federal Republic of Germany
[15] High Energy Physics Laboratory, Institute of Nuclear Physics, Ul. Kawiory 26a, PL-30055 Krakow 30, Poland
[16] Centro Brasileiro de Pesquisas, rua Xavier Sigaud 150, RJ-22290 Rio de Janeiro, Brazil
[17] Université de Paris-Sud, Lab. de l'Accélérateur Linéaire, Bat 200, F-91405 Orsay, France
[18] School of Physics and Materials, University of Lancaster – Lancaster LA1 4YB, UK
[19] LIP, Av. E. Garcia, 14 and Inst. Sup. Te'cnico, Univ. Te'cnica de Lisboa, Av. R. Pais, P-1000 Lisbon, Portugal
[20] Department of Physics, University of Liverpool, P.O. Box 147, GB-Liverpool L69 3BX, UK
[21] LPNHE, Universités Paris VI et VII, Tour 33 (RdC), 4 place Jussieu, F-75230 Paris Cedex 05, France
[22] Department of Physics, University of Lund, Sölvegatan 14, S-22363 Lund, Sweden
[23] Université Claude Bernard de Lyon, 43 Bd du 11 Novembre 1918, F-69622 Villeurbanne Cedex, France
[24] Universidad Complutense, Avda. Complutense s/n, E-28040 Madrid, Spain
[25] Univ. d'Aix – Marseille II – Case 907 – 70, route Léon Lachamp, F-13288 Marseille Cedex 09, France
[26] Dipartimento di Fisica, Università di Milano and INFN, Via Celoria 16, I-20133 Milan, Italy
[27] Niels Bohr Institute, Blegdamsvej 17, DK-2100 Copenhagen 0, Denmark
[28] NIKHEF-H, Postbus 41882, NL-1009 DB Amsterdam, The Netherlands
[29] National Technical University, Physics Department, Zografou Campus, GR-15773 Athens, Greece
[30] Physics Department, University of Oslo, Blindern, N-1000 Oslo 3, Norway
[31] Nuclear Physics Laboratory, University of Oxford, Keble Road, GB-Oxford OX1 3RH, UK
[32] Dipartimento di Fisica, Università di Padova and INFN, Via Marzolo 8, I-35131 Padua, Italy
[33] Depto. de Fisica, Pontificia Univ. Católica, C.P. 38071 RJ-22453 Rio de Janeiro, Brazil
[34] Rutherford Appleton Laboratory, Chilton, GB-Didcot OX11 0QX, UK
[35] Dipartimento di Fisica, Università di Roma II and INFN, Tor Vergata, I-00173 Rome, Italy
[36] CEN-Saclay, DPhPE, F-91191 Gif-sur-Yvette Cedex, France
[37] Istituto Superiore di Sanità, Ist. Naz. di Fisica Nucl. (INFN), Viale Regina Elena 299, I-00161 Rome, Italy
[38] Facultad de Ciencias, Universidad de Santander, av. de los Castros, E-39005 Santander, Spain
[39] Inst. for High Energy Physics, Serpukow P.O. Box 35, Protvino, (Moscow Region), CEI

[40] Institut "Jozef Stefan", Ljubljana, Slovenija
[41] Institute of Physics, University of Stockholm, Vanadisvägen 9, S-113 46 Stockholm, Sweden
[42] Dipartimento di Fisica Sperimentale, Università di Torino and INFN, Via P. Giuria 1, I-10125 Turin, Italy
[43] Dipartimento di Fisica, Università di Trieste and INFN, Via A. Valerio 2, I-34127 Trieste, Italy
and Istituto di Fisica, Università di Udine, I-33100 Udine, Italy
[44] Department of Radiation Sciences, University of Uppsala, P.O. Box 535, S-751 21 Uppsala, Sweden
[45] IFIC, Valencia-CSIC, and D.F.A.M.N., U. de Valencia, Avda. Dr. Moliner 50, E-46100 Burjassot (Valencia), Spain
[46] Institut für Hochenergiephysik, Österr. Akad. d. Wissensch., Nikolsdorfergasse 18, A-1050 Vienna, Austria
[47] Inst. Nuclear Studies and, University of Warsaw, Ul. Hoza 69, PL-00681 Warsaw, Poland
[48] Fachbereich Physik, Universit of Wuppertal, Postfach 100127, W-5600 Wuppertal 1, Federal Republic of Germany

Received 21 May 1992

Abstract. The spectra of prompt electrons and muons from the semi-leptonic decays of heavy hadrons produced in Z^0 decays have been used to measure the coupling of the Z^0 to b quarks weighted by the B hadrons mean semi-leptonic branching fraction, giving a value: $BR^b_{sl} * \Gamma_{b\bar{b}}/\Gamma_H = 0.0221 \pm 0.0015$. The data has also been used to measure the value of the fragmentation parameter, defined in the context of the LUND PS Model, version 7.2, giving: $\varepsilon(b) = \left(8^{+5}_{-3} \pm 2\right) 10^{-3}$. The corresponding value of the mean fraction of the beam energy taken by a B hadron in the fragmentation of a b quark is: $\overline{X^b_E} = 0.69^{+0.02}_{-0.03} \pm 0.01$. If the values of $\Gamma_{b\bar{b}}$ and Γ_H are taken from the Standard Model, the following value is obtained for the mean semi-leptonic braching fraction of B hadrons: $BR^b_{sl} = (10.1 \pm 0.7)\%$. Taking the value of $\Gamma_{b\bar{b}}/\Gamma_H$ from an independent analysis of DELPHI data based on the use of the boosted sphericity product, a value: $BR^b_{sl} = (10.1 \pm 1.3)\%$ is obtained.

1 Introduction

In the Standard Model the Z^0 boson couples with different strengths to up and down type quarks. Experimentally jets produced by heavy quarks are the easiest to isolate because of the use of characteristic properties of heavy hadron production and decay. In the present paper, semi-leptonic decays of B hadrons are used to isolate the Z^0 decays into $b\bar{b}$ pairs. Studying the distributions of the lepton energy and transverse momentum relative to the jet axis allows one to select this channel.

This measurement provides a value for the coupling of the Z^0 to b quarks weighted by the mean semi-leptonic branching fraction of B hadrons. DELPHI has measured previously the fraction of b quarks produced in hadronic events using the distribution of an event shape variable, the boosted sphericity product [1], and also by studying the impact parameter distribution of charged tracks at the level of the beam interaction point [2]. Combining these measurements allows one to give a value for the mean semi-leptonic branching fraction of B hadrons produced in Z^0 decays.

The lepton energy distribution is sensitive to the energy distribution of heavy hadrons and a comparison between data and Monte Carlo simulations allows the fragmentation distributions of the b quark to be studied.

Leptons coming from the decays of charm particles do not have such distinctive features as leptons from direct B decays and with the present statistics only very crude measurements could be extracted on $c\bar{c}$ production. For this reason, in the following analysis, it was assumed that the production of c quarks is given by the Standard Model.

After a description of the event selection and of the aspects of the apparatus that are relevant for this analysis, measurements obtained with selected data samples enriched in muons and in electrons are presented separately and then combined to get the final results.

2 Data and detector

2.1 Event selection and apparatus

For this analysis, the sample of 120 K hadronic events recorded in DELPHI in 1990, were required to fulfill the following selection criteria:

- at least 7 reconstructed charged particles with momentum greater than 100 MeV/c;
- a total charged energy greater than 14% of the centre of mass energy;
- the thrust axis of the event at more than 32° from the beam axis;
- the muon chambers had to be operational for the muon analysis;
- the barrel electromagnetic calorimeter (the HPC) had to be operational for the electron analysis.

The resulting samples of about 100 K events were analyzed for the presence of electron and muon candidates.

To define the solid angle covered by the detectors the following conventions were used. The z axis was taken along the electron beam direction and the y axis was vertical. Polar coordinates of a point in the transverse (x, y) plane were labeled R and Φ. The θ angle was used to define a direction relative to the z axis.

The muon identification relied mainly on the muon chambers, a set of drift chambers providing three dimensional information. In the barrel part of the detector ($52° < \theta < 128°$) there are 3 sets of chambers (see Fig. 1). One set of chambers is located just inside the hadron calorimeter and two sets are just beyond it, with 2 layers

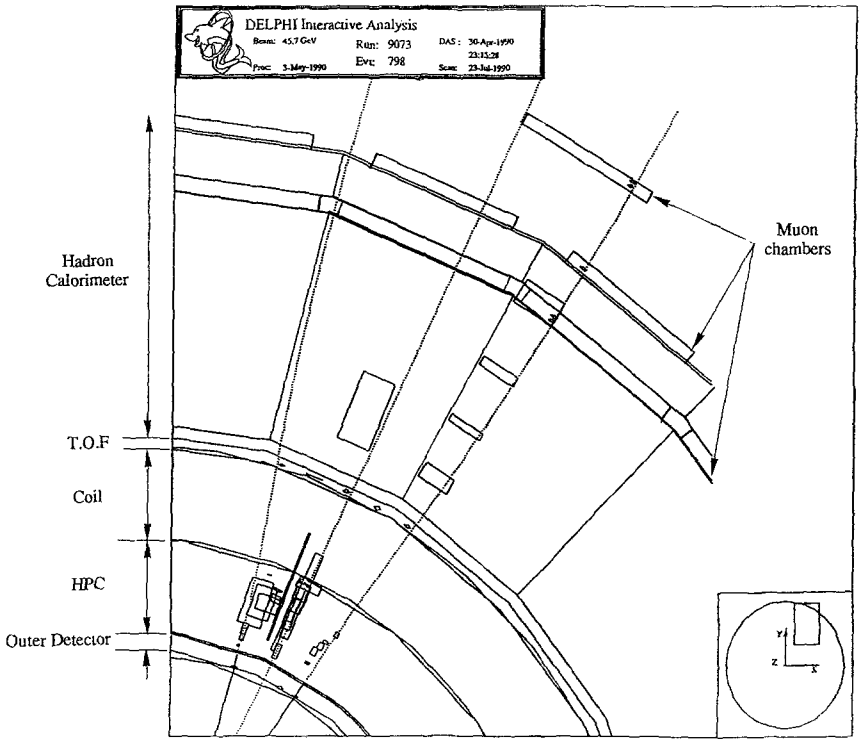

Fig. 1. Display of a part of an event with an identified muon showing the arrangement and the response of the main detector components used in this analysis.

of chambers in each set. The third set, which completes the azimuthal coverage, has a small overlap with the others. The position and the direction of the track are therefore accurately measured in the barrel muon chambers. In the present analysis, only the barrel part of the detector was used, because a better control of the hadronic contamination and a better momentum accuracy was obtained in that region.

The hadron calorimeter (HCAL) was not used, in this analysis, as an active detector to discriminate between muons and hadrons but the different behaviour of these two types of particles in the calorimeter is used to give a measurement of the hadron contamination, by the punch-through mechanism, in the selected sample of muon candidates. The hadron calorimeter is a sampling gas detector incorporated in the magnet yoke, the barrel part covering polar angles from 42.6° to 137.4°, and two end-caps covering polar angles from 11.2° to 46.5° and from 131.5° to 168.8°. The barrel is constructed of 24 sectors, with 20 layers of limited streamer mode detectors inserted into 2 cm slots between the 5 cm iron plates in each sector. The modularity of the end-caps is similar to the barrel, with a sampling depth of 19 layers. The readout boards are segmented into pads which pick up the charges induced by the streamers. Pads are shaped to form towers pointing to the interaction point. The dimensions of a typical tower in the barrel are $25 \times 25 \times 35$ cm^3 and there are four towers along the depth of the calorimeter.

Electron identification relied mainly on the high density projection chamber (HPC), the DELPHI barrel electromagnetic calorimeter covering polar angles between 42° and 138°. It is a gas-sampling calorimeter which uses a long drift time to provide a complete three dimensional charge information in the same way as a time projection chamber. It consists of 144 modules starting at an inner radius R of 208 cm and grouped in 6 azimuthal rings of 24 modules each, with 3 rings on each side of the interaction point along z. Each module subtends 15° in Φ. The thickness of the detector at $\theta = 90°$ is about 17.5 radiation lengths. The electrons released by the ionization of the gas, induced by an electromagnetic shower, drift along the z direction which is parallel to the electric and magnetic fields and are read out by an array of cathode pads. Each shower is sampled nine times in its longitudinal development by the 9 HPC layers of increasing radius. Along the drift direction, the shower is sampled every 3.5 mm and in the $x-y$ plane the charge is collected by pads whose widths range from 2.3 cm in the inner part to 7 cm in the outer part. This excellent granularity allows a very good separation between close particles in three dimensions and hence allows good electron identification even inside jets.

The other detectors that are important in the lepton analysis have been described extensively elsewhere [3], namely the central tracking detectors (inner detector, TPC, and outer detector), which can measure tracks at polar angles larger than 30° with an average momentum resolution $\sigma_P/P \simeq 0.002 \times P$. The time projection chamber (TPC) is the main tracking device. It is a cylinder of 30 cm inner radius, 122 cm outer radius and has a length of 2.7 m. For polar angles between 39° and 141° up to 16 space points can be used. The energy loss (dE/dx) for each charged particle is measured by the 192 TPC sense wires as the 80% truncated mean of the maximum amplitudes of the wire signals and normalized to one for a minimum ionizing particle. In this analysis, when two tracks influence the same wires, the

total energy deposited on these wires contributes to the two dE/dx distributions. In dimuon events, the measured dE/dx resolution is $\pm 5.5\%$. Additional precise $R\Phi$ measurements, perpendicular to the magnetic field, are provided at larger and smaller radii by the outer and inner detectors. The outer detector (OD) has five layers of drift cells at radii between 198 and 206 cm and covers polar angles from 42° to 138°. The inner detector (ID) is a cylindrical drift chamber with an inner radius of 12 cm and outer radius of 28 cm. It covers polar angles between 29° and 151°, and contains a jet chamber section providing $24 R\Phi$ coordinates surrounded by five layers of proportional chambers giving both $R\Phi$ and longitudinal z coordinates.

2.2 Fitting procedure

The signal from B hadron semi-leptonic decays was obtained by evaluating the different contributions to the muon and electron candidate samples separately.

In the following, the procedure applied to the muon sample is explained. The electron analysis differs by a few minor points because of the different origin of non-prompt leptons. These differences are specified in the relevant section.

The muon candidates originate from five different sources:

- prompt muons from the decay of beauty hadrons (B),
- muons from beauty cascade decays (BC),

$$B \to (c \text{ or } \bar{c}) + X \quad \text{and} \quad (c \text{ or } \bar{c}) \to \mu + X,$$
$$B \to \tau + X \quad \text{and} \quad \tau \to \mu + X,$$

- prompt muons from the decay of charm hadrons (C),
- muons from decays in flight of light hadrons (D),
- hadron background (H).

The first component differs from the rest because the transverse momentum of the lepton, relative to the axis of the b quark jet, extends to large values. This difference can be seen directly by measuring the transverse momentum of the lepton relative to the jet direction. For the calculation of this direction the lepton momentum was not included. To suppress spurious fluctuations at large transverse momenta the analysis was restricted to events in which the determination of the direction of the hadronic system was meaningful, i.e. the jet with the lepton had to contain at least one other track of momentum larger than 2 GeV/c. The analysis was performed using the charged particles only, with the help of the jet algorithm defined by the subroutine LUCLUS from the LUND Monte Carlo programs [4], with its default parameters. The estimate of the background contamination is strongly correlated to the signal of prompt muons coming from $c\bar{c}$ events. Thus it was assumed that this $c\bar{c}$ channel is produced according to the Standard Model, as has been verified experimentally [5] albeit with large errors. The contribution from the decays of light hadrons was given by the Monte Carlo simulation.

The two dimensional distribution in P vs P_t of the candidate muons was fitted by minimizing the binned χ^2:

$$\chi^2 = \Sigma (N^\mu - n^\mu)^2 / (N^\mu + n_w^\mu), \tag{1}$$

where N^μ is the number of muon candidates in a bin and n^μ is the sum of the various contributions in that bin, normalized to the total number N_{Z^0} of Z^0 events in the sample:

$$\begin{aligned} n^\mu = N_{Z^0} \times [& \alpha_B \times (n_B^\mu / N_{Z^0}(b\bar{b})) \\ & + \alpha_B \times (n_{BC}^\mu / N_{Z^0}(b\bar{b})) \\ & + \alpha_C \times (n_C^\mu / N_{Z^0}(c\bar{c})) \\ & + \alpha_D \times (n_D^\mu / N_{Z^0}(q\bar{q})) + \alpha_H \times (n_H^\mu / N_{Z^0}(q\bar{q}))], \end{aligned}$$

and n_w^μ is the variance of the number of the expected events, in each bin, from the Monte Carlo simulation. The α_X are the renormalisation coefficients of each muon source X that can be adjusted in the fitting procedure. $n_X^\mu / N_{Z^0}(x\bar{x})$ are the ratios of the number of events accepted in a bin to the total number of events generated in the channel $x\bar{x}$.

To improve the statistical accuracy of the Monte Carlo simulation, additional dedicated samples of events were produced in which each event contained at least one prompt muon of a given source. The normal Monte Carlo sample of events was used to evaluate hadron punch-through and decays of light hadrons.

The numbers $N_{Z^0}(x\bar{x})$ of hadronic Z^0 decays corresponding to each of these samples were normalized so that, if the mean semi-leptonic branching fractions of heavy quarks are the same as in the simulation and if the simulation correctly describes hadron interactions and muon detection efficiencies, all the coefficients α_X will equal unity.

As mentioned previously, the charm contribution coefficient α_C was fixed to unity, the present uncertainties precluding an independent determination of this fraction of the muon signal. The contamination in muons coming from the decays of light hadrons, α_D, was also fixed to the value given by the Monte Carlo simulation. The Monte Carlo simulation was used to predict in each bin the expected number of candidates coming from the various sources. Three parameters were determined from these fits:

- the coefficient α_H of contaminating hadrons,
- the coefficient α_B of prompt muons coming from B decays, directly or through a cascade, with the relative weight of these two components given by the simulation.
- the fragmentation parameter $\varepsilon(b)$ (see Sect. 2.4).

2.3 Monte Carlo simulation of semi-leptonic decays

Simulated hadronic events have been generated using the LUND 7.2 program [4], running in the Parton Shower mode, implemented in DELSIM [6], the DELPHI Monte Carlo simulation program.

The semi-leptonic decays of heavy hadrons, charm and beauty, have been generated using the same program after a retuning of the different branching fractions. The relative contributions from the decays $B \to D \ell \bar{\nu}_\ell$, $B \to D^* \ell \bar{\nu}_\ell$, and $B \to D \pi \ell \bar{\nu}_\ell$ have been taken so that the lepton energy spectrum measured by CLEO at the Υ_{4S} was reproduced [7]. The contribution from non-resonant $D\pi$ decays amounts to 20% of the total of the semi-leptonic decay modes, in this simulation. Data at the Υ_{4S} are not yet accurate enough to give a precise value for this quantity. The value used in the simulation is a mean between theoretical expectations [8] and experimental results.

The semi-leptonic decay channels of charmed mesons and baryons have been introduced in the generator using published data and reasonable theoretical estimates when no data exist or when it was too inaccurate. It has been verified that the lepton energy distributions have similar mean values for all types of weakly decaying charmed hadrons.

The relative contribution of leptons from cascade decays to the total sample of leptons coming from B decays was constrained also by the comparison to CLEO results on the lepton energy distribution. A relative uncertainty of 15% is estimated on this quantity. Electrons and muons from τ lepton decays, where the τ's are produced through the decays of B hadrons, are included in the cascade decays lepton sample.

Leptons from J/ψ decays are considered in the fits as direct leptons from B's but their contribution to the inclusive semi-leptonic branching fraction – of the order of 0.15% – has been subtracted in the final results.

2.4 Monte Carlo simulation of b-quark fragmentation

The energy fraction taken by a B-hadron is partly controlled, in the Monte Carlo simulation, by a fragmentation function which parametrizes the non perturbative aspects of the hadronisation, at the last step of the fragmentation chain, once the radiation of gluons by the quark is completed. The actual fragmentation function to be used depends on the specific Monte Carlo program chosen, and inside the same program it depends on the choice of Λ_{QCD} ($\Lambda_{\mathrm{QCD}} = 260$ MeV was used). The fragmentation of c and b quarks was done using the Peterson et al. distribution [9]:

$$F(z) = A(\varepsilon) \times \frac{1}{z}\left(1 - \frac{1}{z} - \frac{\varepsilon}{1-z}\right)^{-2}, \qquad (2)$$

where $A(\varepsilon)$ ensures* that $\int_0^1 F(z)\,\mathrm{d}z = 1$.

During the simulation of the events, the ε parameter which enters into the expression of $F(z)$ was set to $\varepsilon(b) = 3\ 10^{-3}$ and to $\varepsilon(c) = 24\ 10^{-3}$ for b and c quarks respectively.

The light cone variable z corresponds to $z = \dfrac{E + P_L}{E_0 + P_{L0}}$. The variables entering this expression have been evaluated in the center of mass frame of the string along which is created the heavy particle. For each produced B or D particle, the value of the corresponding z quantity is written on the Monte Carlo simulation output so that, using appropriate weighting procedures, the best values for ε can be determined and other fragmentation distributions could be tested without the need to generate other samples of events.

In the following, given the limited statistics available, only $\varepsilon(b)$ has been fitted and $\varepsilon(c)$ has been assumed to satisfy the relation $\varepsilon(c) = 10 \times \varepsilon(b)$, which is in agreement with the theoretical expectation that $\varepsilon(c) = (m_b/m_c)^2 \times \varepsilon(b)$ [9].

3 Muon identification

The particles considered in this measurement were required to have polar angles θ in the range $-0.6 < \cos\theta < 0.6$ and momenta above 4 GeV/c. For such particles, a fit combining the muon chamber hits with the tracking information was performed in which the tracks were extrapolated to the muon chambers and then associated and fitted to the muon chamber hits. Information from the muon chambers alone allows a measurement of the parameters $R\Phi$, z, θ and ϕ of a track element to be made. The parameters from all possible track elements are then compared to the corresponding parameters of the extrapolated track and a χ^2 test is used to determine the association of the charged track with the muon chambers hits.

In this analysis, in order to accept a track as a muon candidate, the following requirements were imposed:

– the muon candidate must have hits in at least two muon chamber layers, including at least one hit in one of the two external layers,
– the parameters of the track element defined by the muon chambers and the parameters of the extrapolated track, measured in the transverse plane only – $R\Phi$ and ϕ – should give a χ^2 value less than 10. Typical errors for the tracks relevant in this analysis were ± 30 mrad in ϕ and ± 4 cm in $R\Phi$, dominated by the contribution from multiple scattering.

Whenever several tracks could be associated to a given hit in a muon chamber, this hit was attributed to the track which could have the largest total number of associated hits. If an ambiguity remained, the attribution was made according to the global χ^2 which measures the quality of the association between a track and the muon chamber hits.

The reconstruction and identification efficiencies and the contamination from misidentified hadrons could be estimated from the simulation but, in this analysis, we have attempted a direct check of these estimates using the data.

The efficiencies of the muon chambers were monitored by comparing the mean values of the efficiencies

* $A^{-1}(\varepsilon) = \frac{1}{2}\ln\varepsilon + \frac{1}{4-\varepsilon} + \frac{4 - 6\varepsilon + \varepsilon^2}{(4-\varepsilon)\sqrt{\varepsilon(4-\varepsilon)}} \arctan\sqrt{\frac{4-\varepsilon}{\varepsilon}}$

of the 6 layers of chambers in the channel $Z^0 \to \mu^+ \mu^-$. The selection of these events was based on the track multiplicity, required to equal two, and on the momentum, which had to be larger than 35 GeV/c for each track, without considering the activity in the muon chambers. To eliminate the contamination from electron candidates, a positive signal was required in the electromagnetic calorimeter where the deposited energy should be below 2 GeV.

The overall muon identification efficiency was also measured with the $\mu^+ \mu^-$ final state. A mean efficiency

$$\varepsilon_\mu = (78 \pm 2\%) \tag{3}$$

was obtained, which agreed with the estimation from the Monte Carlo simulation program. It was checked with this simulation program that the ambiguities arising from neighbouring tracks do not reduce the identification efficiency inside a jet: the loss of 22% is largely accounted for by the geometrical acceptance of the chambers and the inefficiencies of the selection algorithm.

The purity of the muon candidate sample was determined from the data using three different samples of events:

- τ decays into three charged particles,
- K_s^0 decays into $\pi^+ \pi^-$,
- selected hadrons entering the hadron calorimeter.

The first two samples contain mostly pions and the last one is sensitive also to the contamination from kaons and baryons.

Applying the muon selection criteria to a sample of 1099 charged particles with momentum greater than 4 GeV/c from 3-prong τ decays yielded 14 candidates with a mean energy of 11 GeV. These events are scanned to remove a remaining contamination of 3 events corresponding to the three prongs topology with a muon accompanied by an $e^+ e^-$ pair. The probability for a charged pion to be signed as a muon in this momentum range and topology is therefore

$$\varepsilon(\tau)_\pi^\mu = (1.0 \pm 0.3)\%. \tag{4}$$

(It has been assumed that the behaviour of the few percent of kaons present in the 3-prong τ decays is similar to the behaviour of charged pions.)

The K_s^0 decays into two charged pions provide a measurement of the hadron contamination at lower pion energies. Applying the selection criteria to a sample of 600 such tracks yielded 4 candidates with a mean pion energy of 4.5 GeV, giving

$$\varepsilon(K_s^0)_\pi^\mu = (0.7 \pm 0.3)\%. \tag{5}$$

The response of the hadron calorimeter was studied to measure the hadron contamination at higher momenta. Muon candidates with associated hits in at least three

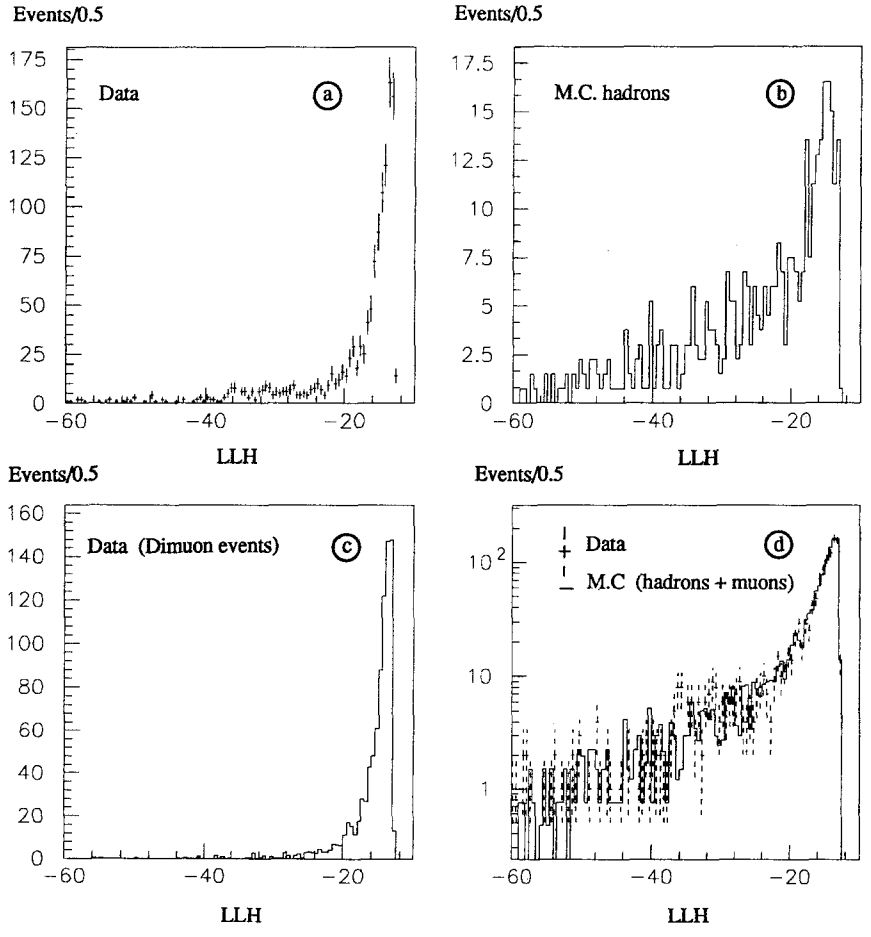

Fig. 2a–d. Log-likelihood distributions (LLH) corresponding to the muon hypothesis for candidate muons signed in the muon chambers and having at least three layers fired in the HCAL: **a** Data; **b** hadrons from Monte Carlo simulation; **c** muons from $Z^0 \to \mu^+ \mu^-$ events; **d** fit of the Data **a** distribution (dotted line) in terms of the two distributions given in **b** and **c** (solid line)

of the four layers of the HCAL were selected. These comprised 85% of the candidates, a very similar fraction in data and in Monte Carlo. Hadrons with momenta larger than 5 GeV/c interacting in the calorimeter could be distinguished from muons by using the energy deposited in each layer of the HCAL (at lower momenta, the energy deposits are too similar). In each layer, a muon gave a signal of about 1.2 GeV (equivalent hadronic energy), distributed according to a Landau-like function which is well represented by the simulation program. From the shape of this distribution, for any given sequence of measured energies E_i in the four HCAL layers, the value of the log-likelihood (LLH) corresponding to the hypothesis that the particle was a muon can be computed. This LLH distribution is shown for all muon candidates in Fig. 2a, and for simulated hadrons in Fig. 2b, for genuine muons selected in $Z^0 \to \mu^+ \mu^-$ events in Fig. 2c. A set of events with very low LLH values, i.e. with very low probabilities for the muon hypothesis, is observed in the first sample. Even for the second sample, consisting of genuine muons, the distribution extends to values smaller than -20. These events correspond to muons developing electromagnetic showers in the calorimeter. But, as expected, the proportion of events with values below -20 is much larger for the third sample, consisting of simulated hadrons because most of them have developed a hadronic shower in the calorimeter.

To determine the hadron contamination, the LLH distribution observed for muon candidates (Fig. 2a) was fitted as the sum of two components, namely the distributions due to hadrons (Fig. 2b) and to real muons (Fig. 2c). Before doing this fit, the energy distribution leading to the LLH distribution for real muons shown in Fig. 2c was corrected, using the Monte Carlo simulation, in order to account for the overlaps inside jets, between muon candidates and neighbouring hadrons (about 20% of muons have at least one cell in the HCAL in common with a hadron). The quality of the final fit is illustrated in Fig. 2d. Considering muon candidates above 10 GeV/c, and normalizing to the total number of hadrons selected in this range, the probability that a hadron will be signed as a muon is:

$$\varepsilon(\mathrm{HCAL})^{\mu}_{\mathrm{had.}} = (0.77 \pm 0.09)\%, \tag{6}$$

where the quoted uncertainty is only statistical. The systematic uncertainty is dominated by the uncertainty on the behaviour of the Monte Carlo prediction for values of LLH higher than -20. As this interval contains only 30% of the hadron candidates, with a momentum larger than 10 GeV/c, it is estimated that the total systematic uncertainty is smaller than 10%. In this momentum range, the additional probability for hadrons to decay and thus to be identified as muons was computed from the Monte Carlo simulation and found to be

$$\varepsilon^{\mu}_{\mathrm{dec.}} = (0.17 \pm 0.04)\%. \tag{7}$$

This gives a total probability for a charged hadron, with a momentum larger than 10 GeV/c, to be identified as a muon of:

$$\varepsilon(\mathrm{had})^{\mu} = (0.94 \pm 0.10)\% \tag{8}$$

in agreement with the value obtained previously from τ decays.

In the following analysis, the energy dependence of the predicted contamination due to hadrons entering the calorimeter was taken from the Monte Carlo simulation but its normalization was taken from the value measured above and imposed as a constraint in the fits with a 20% uncertainty.

4 Electron identification

Only particles inside the full acceptance region of the HPC were considered in the electron analysis. The following selection criteria were imposed:

i) the polar angle θ of the particle relative to the beam direction had to lie in the range 45°–135°,
ii) its impact point in the HPC must not be within $\pm 1°$ of the planes in Φ separating the rows of HPC modules,
iii) its impact point in the HPC had to be at least 4 cm away from the $z = 0$ ($\theta = 90°$) plane,
iv) only particles with momentum between 3 and 30 GeV/c and depositing at least 1 GeV in the HPC were considered. This cut eliminated all minimum ionizing particles, for which the maximum deposited energy is less than 1 GeV, and most low energy electrons produced by gamma conversion.

Two independent means of electron identification were provided by the response of the HPC, and by the energy loss ($\mathrm{d}E/\mathrm{d}x$) measured in the TPC. The calorimetric identification relied on two selections. The first exploited the fine radial segmentation of the HPC. It was based on a χ^2 value which measured the matching between the observed longitudinal shower profile and that of an electron of the same energy. It was defined as

$$\chi^2 = \Sigma_i (F_i - \langle F_i \rangle)^2 / \sigma_i^2, \tag{9}$$

where the sum runs over the nine longitudinal layers of the HPC, F_i is the fraction of the total shower energy deposited in layer i and $\langle F_i \rangle$ and σ_i are the mean and the root mean square of the distribution of the energy fraction deposited in layer i by an electron with energy equal to the shower energy. The values of $\langle F_i \rangle$ and σ_i were determined as a function of the electron energy using pure electron samples provided by the $Z^0 \to e^+ e^-$ and $Z^0 \to e^+ e^- \gamma$ channels, $\tau \to e \nu \bar{\nu}$ decays and photon conversions. This was followed by a selection on the ratio of the total energy in the HPC associated with the track extrapolation, E, to the measured momentum, P: the variable used was

$$\eta = (E/P - \langle E/P \rangle)/\sigma, \tag{10}$$

where the dependence of the mean value $\langle E/P \rangle$ and standard deviation σ of E/P on momentum and shower energy were also determined using the pure electron samples mentioned above.

The second independent means of electron identification was provided by the $\mathrm{d}E/\mathrm{d}x$ measurement in the TPC. The energy loss was defined for tracks having at

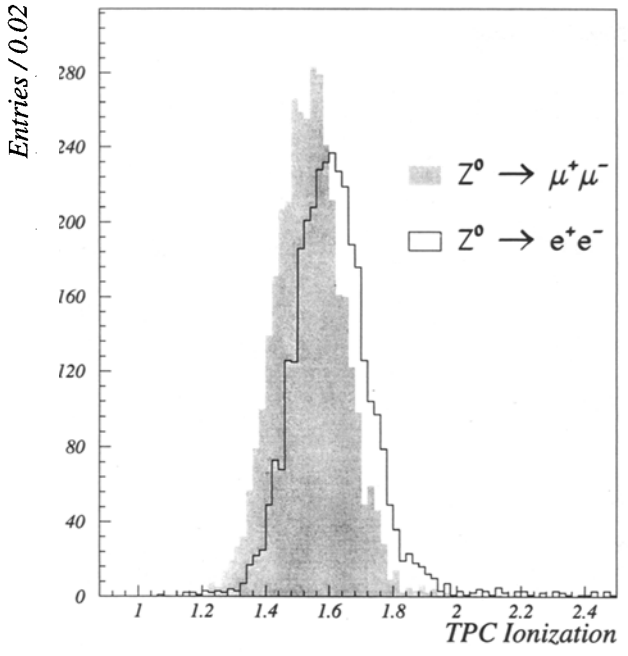

Fig. 3. TPC energy deposit for $Z^0 \to e^+ e^-$ (white area) and $Z^0 \to \mu^+ \mu^-$ events (shaded). The scale was fixed so that the minimum of ionization corresponds to the value 1.0

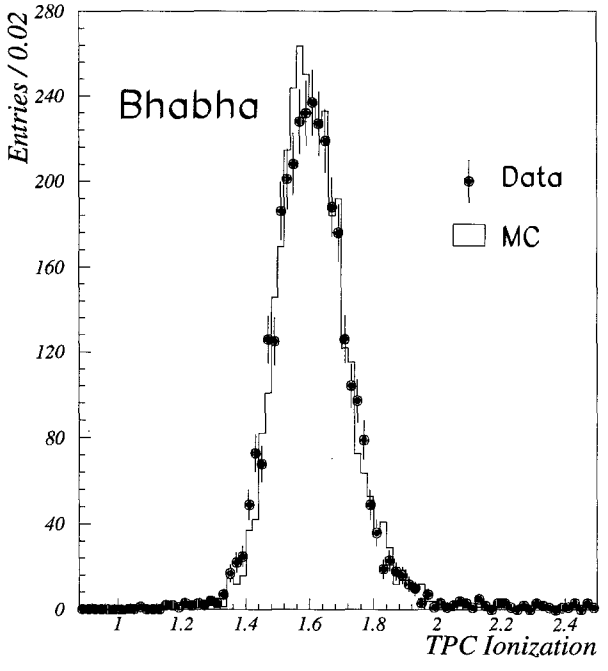

Fig. 4. TPC energy deposit for $Z^0 \to e^+ e^-$ (dots) and Monte Carlo events (line). The scale was fixed so that the minimum if ionization corresponds to the value 1.0

least 100 wires included in the analysis, and the scale was fixed so that the minimum of ionization corresponds to the value 1.0.

The energy loss distribution for electrons on the plateau after the relativistic rise was determined using the $Z^0 \to e^+ e^-$ events and is shown in Fig. 3. The $\mathrm{d}E/\mathrm{d}x$ response for real muons obtained from $Z^0 \to \mu^+ \mu^-$ events is also shown in the same figure. The electron

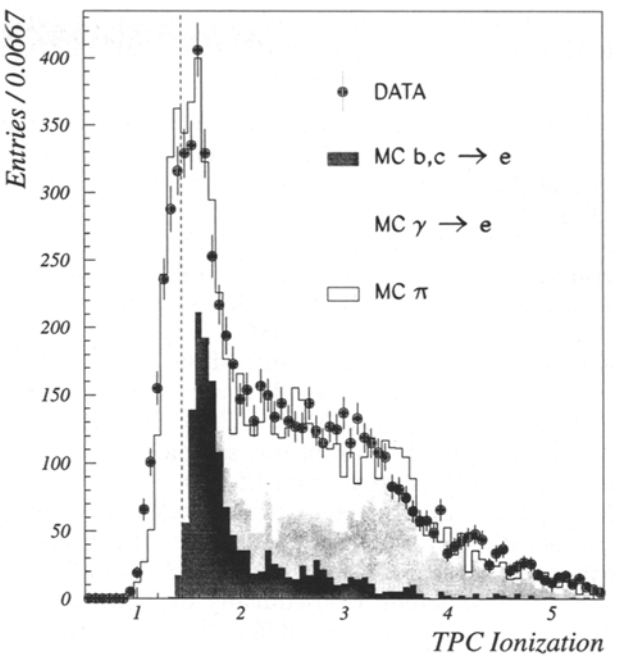

Fig. 5. TPC energy deposit for an electron enriched $q\bar{q}$ sample: a vertical dashed line divides BCKG from SIGNAL. Only tracks with more than 50 $\mathrm{d}E/\mathrm{d}x$ measurements are plotted. The scale was fixed so that the minimum of ionization corresponds to the value 1.0

peak has a standard deviation of 7% and its mean value is clearly above that of the muon peak even at this high momentum. The $\mathrm{d}E/\mathrm{d}x$ distributions in $e^+ e^-$ events in the real data and in the Monte Carlo simulation are compared in Fig. 4 and agree well. For tracks in jets the $\mathrm{d}E/\mathrm{d}x$ measurement is more difficult due to presence of nearby tracks, but nevertheless the Monte Carlo still compares well with the data. This is shown in Fig. 5, which compares the $\mathrm{d}E/\mathrm{d}x$ distributions for an electron enriched track sample from $q\bar{q}$ events in the data (dots) and in the Monte Carlo simulation (line).

The redundancy of these two selections, using the HPC and the TPC respectively, allowes one to estimate independently from Monte Carlo both the electron identification efficiency and the contamination from misidentified hadrons. Monte Carlo events were used only to check the reliability of the method. The procedure relies on the fact that even in $q\bar{q}$ events it is still possible to select a sample of hadrons with negligible electron contamination by requiring $\mathrm{d}E/\mathrm{d}x < 1.43$, as shown in Fig. 5. In the momentum region of interest, the values for electrons are always distributed about the plateau position while for hadrons and muons the mean value is lower, in the relativistic rise region. When the ionization samples of two overlapping tracks are attributed to a single track, as may happen in jets, the measured $\mathrm{d}E/\mathrm{d}x$ value is higher than the true one. This is the origin of the tail at high $\mathrm{d}E/\mathrm{d}x$ that is present in the $q\bar{q}$ data of Fig. 5 but was not seen in the $e^+ e^-$ and $\mu^+ \mu^-$ data. Thus the TPC information can be used to divide all tracks selected according to criteria *i–iv* into two samples:

– SIGNAL, defined by $dE/dx > 1.43$ (or unmeasured);
– BCKG, defined by $dE/dx < 1.43$; this sample has an electron contamination below 1%.

The BCKG sample can then be used to estimate the electron content of the SIGNAL sample simply by weighting the BCKG events and subtracting them from the SIGNAL, the remainder being the electrons present in the SIGNAL distribution. The weights needed were determined as a function of momentum P and transverse momentum P_t from the SIGNAL/BCKG ratio observed in a sample selected using the HPC only. This sample consisted of the tracks which satisfied the first three criteria *i–iii* but gave only a small energy deposit in the HPC ($E_{\mathrm{HPC}} < 1$ GeV). The Monte Carlo indicates that the electron contamination in this sample is 0.6%. The values of the weights range from 1.5 to 4.

Monte Carlo events were used to check this method. The application of the dE/dx cut causes the P and P_t distributions of the hadrons in the SIGNAL and BCKG samples to be different. Consequently their unweighted E/P and η distributions also differ. Figure 6 compares (a) the E/P and (b) the η distributions of Monte Carlo hadrons falling in the two samples after applying these weights. The agreement is good in all the momentum regions.

The electron candidates were selected by the criteria *i–iv* and by requiring

– $dE/dx > 1.43$ ('SIGNAL'),
– $\chi^2 < 20$ and $\eta > -2.0$.

Monte Carlo estimates show that less than 2% of the original electrons were lost by the dE/dx cut. Figure 7a

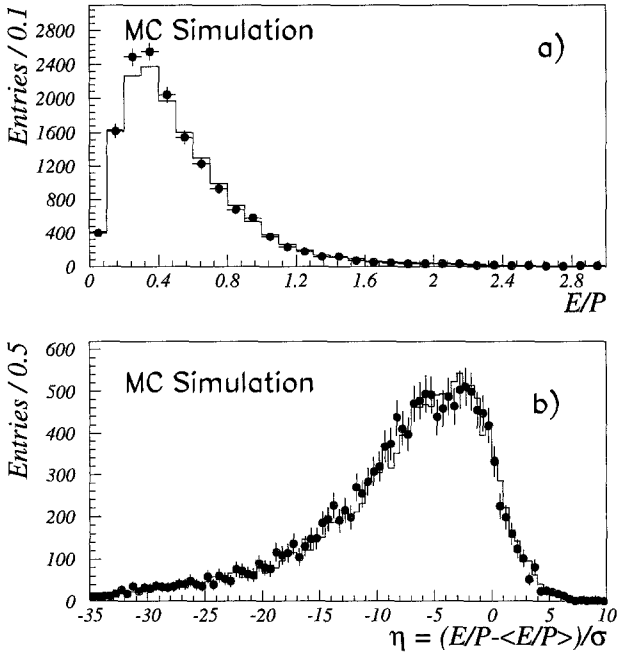

Fig. 6a, b. E/P ratio for generated hadrons falling in the SIGNAL sample (line) and in the weighted BCKG one (MC events) **a**; same for $\eta = \frac{E/P - \langle E/P \rangle}{\sigma}$ **b**

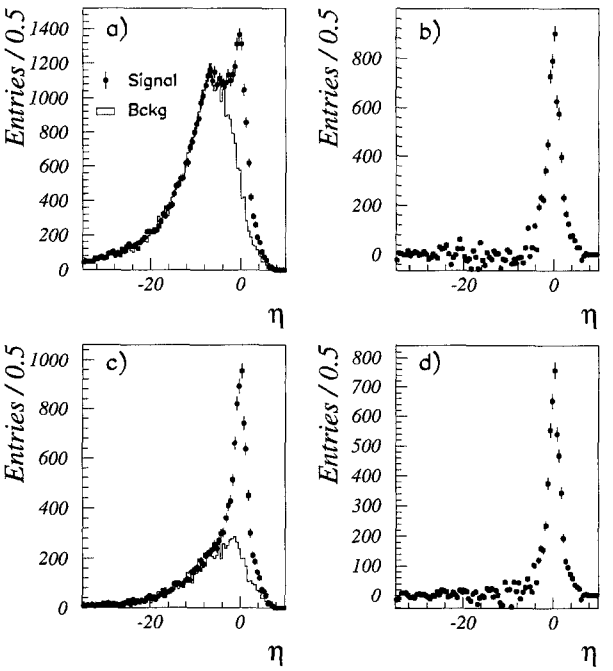

Fig. 7a–d. η distribution of data for SIGNAL (dots) and BCKG (line) samples, before **a** and after **c** χ^2 cut; data residual distributions before **b** and after **d** cut

and c show the η distribution for tracks in the SIGNAL sample (data points) and the weighted BCKG sample (line) before and after applying the $\chi^2 < 20$ cut. The efficiency of the χ^2 cut can be evaluated by comparing the subtracted distributions before and after applying it, shown in Figs. 7b and 7d. The efficiency of the η cut is given by the fraction of the events in the subtracted distribution after the χ^2 cut that pass the η selection. For the chosen cut at $\eta > -2.0$ this efficiency is $\varepsilon^{\eta} = (0.843 \pm 0.005)$ in good agreement with the Monte Carlo prediction $\varepsilon^{\eta}_{\mathrm{mc}} = 0.854$. In the Monte Carlo simulation, the number of electrons found with this procedure in the region $\eta > -2$ agreed with the true number within 2%. The electron identification efficiency after applying both the η cut and the χ^2 cut was estimated to be

$$\varepsilon^{\chi^2+\eta} = (0.68 \pm 0.01), \tag{11}$$

where the error is dominated by the systematics of the subtraction procedure. It is lower than the MC prediction $\varepsilon^{\chi^2+\eta}_{\mathrm{mc}} = (0.77 \pm 0.01)$. The difference is due mostly to an approximate description of the regions near the gaps between the HPC modules along the z direction. The overall electron identification efficiency is

$$\varepsilon_e = (0.58 \pm 0.03). \tag{12}$$

The above value takes into account the efficiency for associating an electron track to its HPC shower (0.85 ± 0.03). This last number, giving the largest contribution to the overall error, has been experimentally determined using e^+e^- and $e^+e^-\gamma$ samples. It has been verified that this efficiency is almost momentum independent by using Monte Carlo events, and by applying the procedure to the data for different momentum intervals.

The hadron contamination h_{cont}, defined as the fraction of selected particles which were really hadrons, can be measured by counting the number of weighted BCKG events passing all the HPC cuts. It was found to be $h_{cont}=0.374\pm0.019$. The error quoted is dominated by the systematic uncertainties. The corresponding probability that a hadron in the selected momentum range would be identified as an electron is

$$\varepsilon_h^e=(1.13\pm0.06)\,10^{-2}. \quad (13)$$

The 5% uncertainty is due to the following sources: $\pm3.6\%$ statistical, $\pm4\%$ weighting systematics, $\pm1\%$ electron presence in BCKG sample. The systematic error due to the weighting procedure was evaluated normalizing the weighted distribution of the BCKG sample in different intervals of the η distribution outside the electron region.

The efficiency of the selection criteria and the purity of the electron sample were also measured using two different event samples:

- photons converted in the material before or at the entrance wall of the TPC
- K_S^0 decays into two pions

The first sample of events contains essentially only electrons and the second only pions with a contamination from electrons estimated from Monte Carlo to be 0.7%. The P and P_t distributions of both samples were well reproduced by the DELPHI simulation. Of the about 500 real electrons satisfying criteria *i–iv*, a fraction 0.72 ± 0.02 were found to pass the η and χ^2 selections. This has to be compared with a Monte Carlo simulation prediction of 0.83 ± 0.02. This confirms the previous conclusion that the χ^2 selection is less efficient in the data than in the Monte Carlo.

From a sample of 1500 pions from real K_S^0 decays, satisfying criteria *i–iii*, the probability for a charged pion to be misidentified as an electron is found to be

$$\varepsilon(K_s^0)_\pi^e=(1.8\pm0.4)\,10^{-2} \quad (14)$$

compatible with the more precise measurement given before. The mean pion energy of this sample is 3.5 GeV.

The background from photon conversions was reduced by removing the electron candidates which have $dE/dx>2.4$ and are compatible with forming a secondary vertex with any oppositely charged particle. This cut removed about 60% of the electrons from gamma conversion. The fraction of V° candidates removed by this cut and the shapes of their P and P_t distributions were well reproduced by the Monte Carlo simulation. It was estimated that 7% of electrons from b decay are lost by this cut.

5 Measurement of $BR_{sl}^b * \Gamma_{b\bar{b}}/\Gamma_H$ and $\varepsilon(b)$ with the muon sample

The P vs P_t distribution of prompt muon candidates as given by the Monte Carlo simulation and corresponding to a fixed value of the fragmentation parameter $\varepsilon(b)$, has been compared to the corresponding distribution of the 4040 muon candidates selected in the data.

To determine the value for $\varepsilon(b)$, a sample of 2081 candidates enriched in prompt muons from B decays has been selected by taking events with a transverse momentum larger than 1 GeV/c. The variation of the χ^2 of the fit is used to determine the favoured range of values for $\varepsilon(b)$:

$$\varepsilon(b)=\left(9\,^{+5}_{-4}\right)10^{-3}. \quad (15)$$

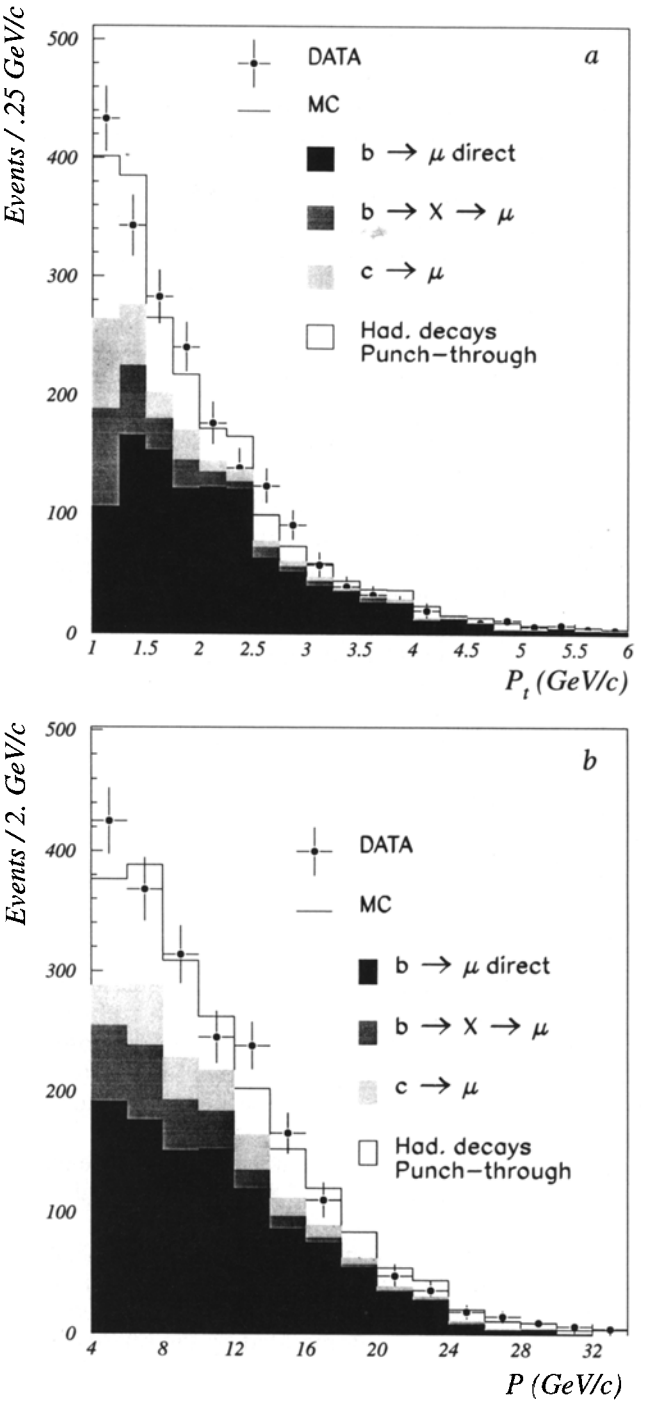

Fig. 8a, b. Projections of the P_t vs P fitted bidimensional distribution showing the amplitude of the various components in the sample of muon candidates. **a** P_t distribution, **b** P distribution

Table 1. Composition of the muon sample, as defined in Sect. 2.2

	B	*BC*	*C*	*H*	*D*
Relative fraction (%)	54±3	12±1	10	16±2	8

From the parameters used in the Monte Carlo simulation, the corresponding range of variation for the mean beam energy fraction taken by a *B*-hadron is then:

$$\overline{X_E^b} = 0.685 \begin{matrix} +0.018 \\ -0.020 \end{matrix}. \quad (16)$$

In Fig. 8a and b are given the projections along P and P_t respectively of the measured and fitted P vs P_t muon distribution.

Taking the central value for $\varepsilon(b)$ and considering that the uncertainty on this quantity contributes to the statistical uncertainty, the rate of prompt muons coming from B hadron semi-leptonic decays in Z^0 events is measured to be:

$$BR_{sl}^b * \Gamma_{b\bar{b}}/\Gamma_H = 0.0229 \pm 0.0017. \quad (17)$$

The corresponding value for the fitted parameter α_B is $\alpha_B = 1.051 \pm 0.066 \pm 0.045$. The second of the uncertainties on α_B comes from the variation of $\varepsilon(b)$.

The fitted value of α_H is 0.84 ± 0.10, indicating a hadron contamination 16% smaller than expected from the evaluation given in Sect. 3 which was used to normalize the predicted contamination. This number in fact includes also possible deviations in hadronic, charm and cascade decays from the contributions assumed for these components in the simulation. The χ^2 of the fit is equal to 94 for 63 degrees of freedom. But, in the region $P_t > 1$ GeV/c, which contains most of the leptons from B hadrons decays, the χ^2 of the fit is equal to 43 for 39 degrees of freedom; the corresponding sample composition is given in Table 1.

5.1 Study of systematic uncertainties

The same analysis was repeated varying by one standard deviation the parameters kept fixed in the fit and varying also the limits and the conditions of the fit. The observed variation on α_B is taken as an estimate of the systematic unvertainty on this parameter. The results are summarized in Table 2.

The total relative systematic uncertainty on the quantity $BR_{sl}^b * \Gamma_{b\bar{b}}/\Gamma_H$ amounts to 4.8%. Each contribution to Table 2 is detailed below.

The mean semi-leptonic branching fraction in $c\bar{c}$ events used in this analysis was: $BR_{sl}(c \to \mu) = (10.0 \pm 1.1)\%$ computed from an average of published [10] values. Its uncertainty is dominated by the relative error on the best measured of these quantities, the value obtained for the D^+, which amounts to 9%. The value used for the semi-leptonic branching fraction of any other charmed particle was obtained by scaling the value quoted for the D^+ by the ratio of the lifetimes of this charmed particle and of the D^+. The rate of charmed baryons production was allowed to vary by a factor of two and an uncertainty of 20% was assigned to the rate of D^* relative to prompt D production. The effect of the recent [11] increase of the measured branching fraction of the D^{*+} into $D^0\pi^+$ was also included.

Table 2. Systematic uncertainties in the muon sample

Parameter	Relative or absolute variation	Relative variation on $BR_{sl}^b * \Gamma_{b\bar{b}}/\Gamma_H$ (%)
Direct charm	11.0%	0.3
Secondary charm	15.0%	1.5
Decays of light hads.	10.0%	0.7
Efficiency of μ id.	3.0%	3.0
Evaluation of $\varepsilon(b)$	$2\ 10^{-3}$	2.2
Min. bin content	5 to 25 counts	1.0
P_t definition		2.0

As indicated in Sect. 2.3, the fraction of leptons from B cascade decays, relative to the production of direct leptons from B's, was constrained to reproduce the inclusive lepton energy distribution measured by the CLEO experiment [7]. If it is assumed that the inclusive direct semi-leptonic branching fraction for B^0 and B^+ mesons is equal to 10% it is found that $BR_{sl}(b \to c \to \mu) = (9.1 \pm 1.5)\%$.

The uncertainty on the absolute value of the identification efficiency for muons, 3%, has been included to account for remaining differences between data and the Monte Carlo simulation on the behaviour of the detectors and of the passage of muons through the calorimeters.

The systematic uncertainty on $\varepsilon(b)$ was taken to be $\pm 2\ 10^{-3}$ and it corresponds to a variation of ± 0.015 on $\overline{X_E^b}$. It has been obtained by repeating the measurement of $\varepsilon(b)$ described previously after a change of the fractions of cascade muons, muons from charm and decays of light hadrons by one sigma.

The stability of the results has been verified by changing the conditions of the fit. The minimum muon momentum was varied from 3 GeV/c to 5 GeV/c and the minimum number of events required to include a given bin in the P_t vs P distribution was changed from 5 to 25. In these fits the bin size was not constant because at large P_t and P several bins have been grouped together. The bin contents that are below a given threshold value have been added together and this final value was compared to the corresponding Monte Carlo expectation and included in the χ^2 evaluation.

Finally, it has been also verified that the result did not depend on the definition of the jet axis used to compute the muon transverse momentum. The same measurement was repeated, using simply the muon transverse momentum relative to its jet axis, without the 2 GeV requirement on the minimum hadronic energy previously imposed on the other charged tracks present in the jet.

6 Measurement of $BR^b_{sl} * \Gamma_{b\bar{b}}/\Gamma_H$ and $\varepsilon(b)$ with the electron sample

The cuts discussed in Sect. 4 selected 5041 electron candidates. The same cuts were also applied to the different Monte Carlo samples, for which the electron identification efficiency and the hadron contamination were rescaled to the values obtained for the data. As in the muon case, five different sources contribute to the selected sample. The first three (B, BC, C) are the same as in the muon case, while other electrons come from Dalitz decays of the π^0, γ conversion (D) and from misidentified hadrons (H). It was checked using the reweighted BCKG sample that the shape of the P and P_t spectra of the misidentified hadrons present in the selected sample was correctly reproduced by the Monte Carlo simulation, (see Figs. 9a, b). To increase the statistical significance of the Monte Carlo simulation, dedicated samples were again used for the first three candidate sources. All samples were then normalized to the total number of Z^0 decays in the data. As before, the renormalisation coefficient α_X of each electron source was obtained by fitting the two-dimensional distribution in P_t and P. Also as before, α_H and α_D should equal unity if the understanding of the hadron contamination and photon conversions is correct and α_C was fixed to unity. A further parameter, left free to vary in the fit, was the fragmentation parameter $\varepsilon(b)$. At each step of the minimization, electrons from heavy flavour decay were reweighted according to their z value to match the new $\varepsilon(b)$ value, to allow the best value of this parameter to be determined. In a first stage the full P and P_t range was fitted letting α_B, α_H, α_D and ε_B free, in order to measure the hadron contamination independently from the analysis of Sect. 4. The fit gave:

$$\alpha_D = 1.62 \pm 0.20, \tag{18}$$

$$\alpha_H = 0.96 \pm 0.10 \tag{19}$$

(so confirming the hadron background estimate, while the Monte Carlo simulation underestimates the number of electrons coming from photon conversion, as already noticed in [12]), and:

$$\varepsilon(b) = \left(6.8 \begin{smallmatrix} +7.8 \\ -3.3 \end{smallmatrix}\right) 10^{-3}, \tag{20}$$

$$\alpha_B = 0.97 \pm 0.09, \tag{21}$$

$$\chi^2/Ndf = 91/107, \tag{22}$$

which correspond to

$$BR^b_{sl} * \Gamma_{b\bar{b}}/\Gamma_H = 0.0211 \pm 0.0019, \tag{23}$$

$$\overline{X^b_E} = 0.694 \begin{smallmatrix} +0.032 \\ -0.019 \end{smallmatrix}. \tag{24}$$

To check the fit stability α_H was fixed to unity and the fit performed in the region $P_t > 1$ GeV/c, which is enriched in electrons coming from B decays, with α_B, α_D and $\varepsilon(b)$ allowed to vary. The following result was obtained:

$$BR^b_{sl} * \Gamma_{b\bar{b}}/\Gamma_H = 0.0205 \pm 0.0022, \tag{25}$$

$$\varepsilon(b) = \left(7.1 \begin{smallmatrix} +8.8 \\ -4.1 \end{smallmatrix}\right) 10^{-3}, \tag{26}$$

$$\chi^2/Ndf = 74/83. \tag{27}$$

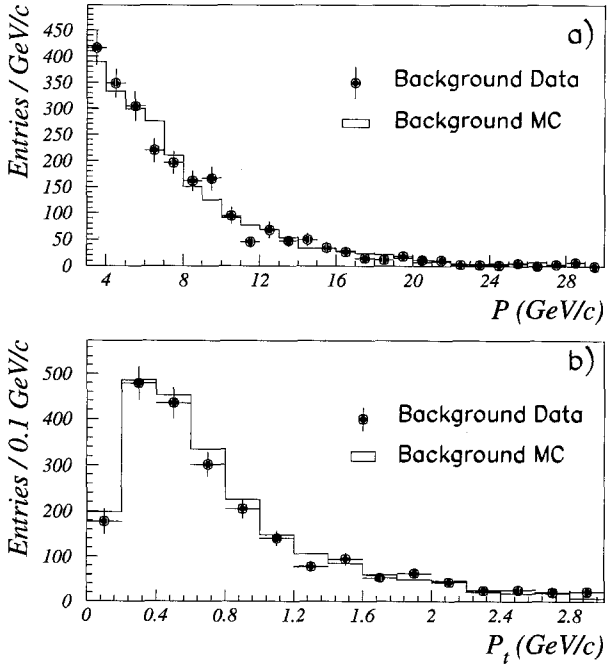

Fig. 9a, b. Data (cross) P **a** and P_t **b** BCKG sample reweighted. Superimposed line shows Monte Carlo prediction for the background shape. P_t is computed without removing the track from the jet

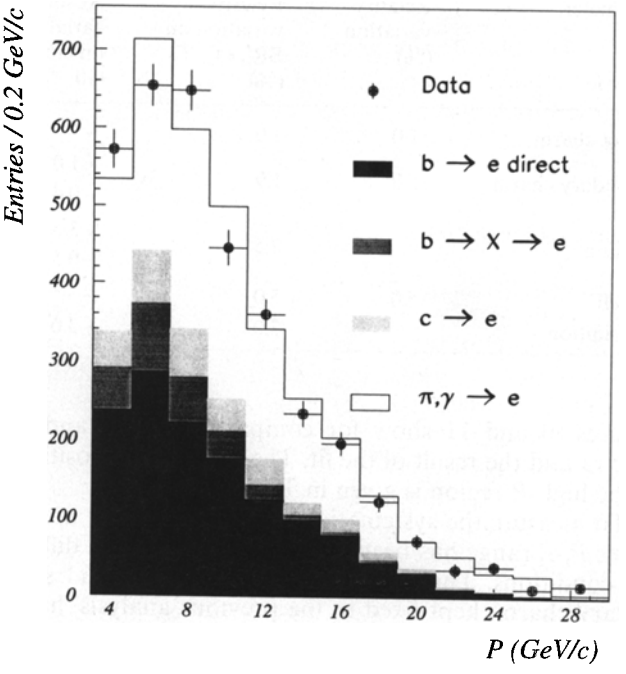

Fig. 10. P composition of electron candidates, after a $P_t > 1$ cut

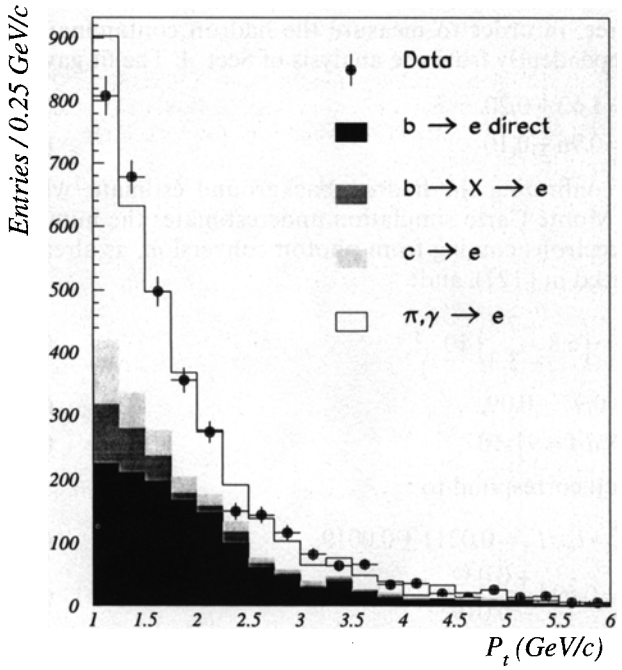

Fig. 11. P_t composition of electron candidates. P_t is computed removing the track from the jet

Table 3. Composition of the electron sample, as defined in Sect. 2.2

	B	BC	C	H	D
Relative fraction (%)	38 ± 3	8 ± 1	9	33 ± 3	12 ± 2

Table 4. Systematic uncertainties in the electron sample

Parameter	Relative variation (%)	Relative variation on $BR^b_{sl} * \Gamma_{b\bar{b}}/\Gamma_H$ (%)	Absolute variation on $\varepsilon(b)$ (10^{-3})
Direct charm	11.0	1.0	–
Secondary charm	15.0	1.9	$^{+1.0}_{-0.4}$
Binning		2.5	$^{+3.5}_{-0.5}$
e id eff	5.0	5.0	–
P_t definition		3.0	+3.0

Figures 10 and 11 show for comparison the P_t and P spectra and the result of the fit. The sample composition in the high P_t region is given in Table 3.

To measure the systematic uncertainties the fit in the wider P, P_t range has been repeated under several different conditions. The contributions from direct and secondary charm, kept fixed in the previous analysis, have been varied by plus or minus one standard deviation. The bin size has been reduced (in such a way to have always at least 6 events per bin, and 111 bins) and increased (up to a limit of at least 20 events per bin and 79 bins). Combined with the quoted error on the electron identification efficiency, the overall systematic error is $\pm6.7\%$ for $BR^b_{sl} \times \Gamma_{b\bar{b}}/\Gamma_H$ and $\binom{+4.7}{-0.6} 10^{-3}$ for $\varepsilon(b)$. Individual contributions are reported in Table 4.

7 Measurement of the mean B semi-leptonic branching fraction

From the spectra of prompt muons and electrons generated in the semi-leptonic decays of the b quark the following results have been obtained:

$$\mu\text{: } BR^b_{sl} * \Gamma_{b\bar{b}}/\Gamma_H = 0.0229 \pm 0.0017(\text{stat.}) \pm 0.0011(\text{syst.}), \quad (28)$$

$$e\text{: } BR^b_{sl} * \Gamma_{b\bar{b}}/\Gamma_H = 0.0211 \pm 0.0019(\text{stat.}) \pm 0.0014(\text{syst.}), \quad (29)$$

so that:

$$\mu + e\text{: } BR^b_{sl} * \Gamma_{b\bar{b}}/\Gamma_H = 0.0221 \pm 0.0015. \quad (30)$$

If, as in other measurements [13], the value of $\Gamma_{b\bar{b}}/\Gamma_H = 0.218$, as given by the Standard Model, is used, the inclusive semi-leptonic branching fraction of B hadrons deduced from the present measurements is:

$$BR^b_{sl} = (10.1 \pm 0.7)\%. \quad (31)$$

In a companion paper [1] the ratio $\Gamma_{b\bar{b}}/\Gamma_H$ was measured using an event shape variable, the Boosted Sphericity Product:

$$\Gamma_{b\bar{b}}/\Gamma_H = 0.219 \pm 0.014 \pm 0.019. \quad (32)$$

From this measurement, combined with the present result, the value for the mean semi-leptonic branching fraction of B mesons in Z^0 decays can be derived from DELPHI data:

$$BR^b_{sl} = (10.1 \pm 1.3)\%. \quad (33)$$

The most precise determination of the semi-leptonic branching fractions for B particles was obtained at the $\Upsilon(4S)$ and is $(10.3 \pm 0.4)\%$ [14]. At LEP, B^0_s and B baryons are produced in addition to B^0_d and $B^{\pm}$. As a result, the mean semi-leptonic branching fraction measured at the Z^0 may differ from the value obtained at the $\Upsilon(4S)$. However, current expectations on the hierarchy of B particle lifetimes are such that the mean semileptonic branching fraction observed at LEP should be very close or slightly smaller than the $\Upsilon(4S)$ one. The present result agrees with these expectations.

8 Conclusions

The spectra of prompt muons and electrons from the semi-leptonic decays of heavy hadrons produced in hadronic Z^0 decays were obtained. From them, the coupling of the Z^0 to b quarks weighted by the mean B hadrons

semi-leptonic branching fraction into muons or electrons has been derived:

$$BR_{sl}^{b} * \Gamma_{b\bar{b}}/\Gamma_H = 0.0221 \pm 0.0015. \quad (34)$$

The parameter $\varepsilon(b)$ of the Peterson fragmentation function, in the framework of a Monte Carlo simulation which uses the LUND-PS (7.2) program with $\Lambda_{QCD} = 260$ MeV, is $\left(8^{+5}_{-3} \pm 2\right) 10^{-3}$ from the combined measurement using the samples of selected electrons and muons.

The corresponding mean beam energy fraction taken by a B hadron amounts to:

$$\overline{X_E^b} = 0.69^{+0.02}_{-0.03} \pm 0.01 \quad (35)$$

Acknowledgements. We are greatly indebted to our technical collaborators and to the funding agencies for their support in building and operating the DELPHI detector, and to the members of the CERN-SL Division for the excellent performance of the LEP collider. We thank T. Sjöstrand for fruitful discussions.

References

1. DELPHI Collab., Measurement of the Z^0 Branching Fraction to b quark pairs using the Boosted Sphericity Product, CERN-PPE/92-007, subm. to Phys. Lett. B
2. DELPHI Collab., P. Abreu et al.: Z. Phys. C – Particles and Fields 53 (1992) 567
3. DELPHI Collab.: Nucl. Instrum. Methods A 303 (1991) 233
4. T. Sjöstrand: Comput. Phys. Commun. 27 (1982) 243; ibid. 28 (1983) 229; T. Sjöstrand, T. Bengtsson: Comput. Phys. Commun. 43 (1987) 376
5. DELPHI Collab., P. Abreu et al.: Phys. Lett. B252 (1990) 140
6. DELSIM Reference Manual: DELPHI 87-98 PROG 100, Geneva, 1989
7. D.G. Cassel, CLEO Collab.: in: Physics in Collisions 10, p. 276. A. Goshow, L. Montanet (eds.). Gif sur Yvettes: Editions Frontières 1990
8. N. Isgur, D. Scora, B. Grinstein, M.B. Wise: Phys. Rev. D39 (1989) 799; E. Golowich et al.: Z. Phys. C – Particles and Fields 48 (1990) 89
9. J. Oliensis: Phys. Rev. D23 (1981) 1431; C. Peterson et al.: Phys. Rev. D27 (1983) 105
10. Particle Data Group: Phys. Lett. B239 (1990) 1
11. R. Kass: International Symposium on Heavy Flavour Physics, Orsay, 1991
12. DELPHI Collab., P. Abreu et al.: Z. Phys. C – Particles and Fields 53 (1992) 555
13. L3 Collab., B. Adeva et al.: Phys. Lett. B241 (1990) 416; Phys. Lett. B261 (1991) 177; ALEPH Collab., D. Decamp et al.: Phys. Lett. B244 (1990) 551; OPAL Collab., M.Z. Akrawy et al.: Phys. Lett. B263 (1991) 311
14. K. Berkelman, S.L. Stone: Preprint CLNS 91-1044, to be published in Annual Review of Nuclear and Particle Science